Daily Science Report
Stratus2007 Cruise
NOAA Ship Ronald H. Brown
C. W. Fairall (NOAA/ESRL) and R. A. Weller (WHOI)
Report #5 October 22, 2007

Summary of Recent Activities

The ship departed Panama as planned the morning of October 16. Observations were officially begun on October 18. The ship reached 20 S 75 W by the end of October 22 (Fig. 1). The ESRL observations include air-sea fluxes/near-surface bulk meteorology, cloud ceilometers, radar wind profiler, scanning Doppler C-band precipitation radar, a microwave radiometer for column water vapor/liquid, and aerosols in the 0.1 to 6 micrometer range. Rawinsonde launches were every 6 hours until reaching the buoy location at 20 S 85 W when the frequency was increased to every 4 hours (beginning 0000GMT on Oct 23). A sample rawinsonde profile is shown in Fig. 2; a strong subsidence inversion typical of stratocumulus regions is visible at a height of about 900 m. This trace indicates a cloud with a base at about 800 m. Fig. 3 is a photograph taken at the same time as the sounding. Another interesting feature is the very strong wind shear at the inversion. The cloud ceilometer return for the day is shown in Fig. 4. A brief clear period is visible at 1700 and the cloud base actually decreases after arrival at the buoy.

Cloud top and bottom heights are critical in assessing bulk cloud properties that are of interest in characterizing important cloud characteristics (cloud thickness, optical thickness, liquid water path). A modern radiosonde profile is good for getting cloud top height in stratocumulus conditions but is fairly poor at estimating cloud bottom height. Also, it is difficult to get more than 6 sonde estimates a day. Remote sensors offer the capability for near-continuous estimates of the heights. In Fig. 5 we show an example from Oct. 22 using the ceilometer to estimate cloud bottom height and a Doppler wind profiling radar to estimate cloud top height. In this case the ceilometer cloud base heights are plotted on the profiler backscatter intensity (return signal to noise ratio, SNR). The profiler backscatter is enhanced by the strong humidity gradient at the top of the marine boundary layer. In the figure this enhancement is clearly visible as the bright region at 1 km just above the black dots (ceilometer cloud base). The bright region near the surface is an artifact caused by scattering from the sea surface. For this day, we see a thickening of the cloud the last few hours of the day, roughly corresponding to arrival at the buoy. Note the thickening is associated with lowering of cloud base; cloud top stays roughly constant.

Data from the aerosol system are shown in Fig. 6. In this case we show data from the transect from the Gulf of Panama to 20 S (290 to end of 295). Note the lowest aerosol concentrations in the precipitation region of the Gulf of Panama; the high values off N. Peru (about 300/cm^3) are typical of larger values usually found at the WHOI buoy site. A general trend appears in the transect south with the number of smaller particles

increasing after a minimum on JD 293 but the number of larger particles is decreasing (possibly because of the lower wind speeds the last few days). However, on our arrival at the DART buoy site, aerosol concentrations dropped abruptly. This drop is associated with a 'pocket of open cells' (POC) cloud spatial structure that was visible on satellite images.

The 'coast hugging' nature of this year's transect south is new this year and it provides a unique snapshot of the spatial structure of the atmosphere off S. America. We are presently working on some preliminary evaluations of these data but a few hints of the results are already available. Fig. 7 displays a longitude-height cross section from the rawinsonde data. The deepening of the boundary, intensification of the lower tropospheric thermal gradient, and rapid drying of the troposphere as we go away from the equator are striking. Fig. 8 shows a time-height cross section of cloud base height for the same period (sorry for mixing time and latitude plots but things are primitive out here), which shows the increase in boundary layer height is approximately matched by an increase in cloud base (i.e., roughly constant cloud thickness) until the end of the transect. Finally, Fig. 9 shows the behavior of the near-surface meteorological variables on the transect. Air-sea temperature difference remained small throughout the upwelling region (S of 5 S), sensible heat flux is near zero and latent heat flux fairly features at about 50 W/m^2 (significantly lower than typical values at the WHOI buoy this time of year).

Major oceanographic activities include deployment of surface velocity and SST drifters and profiling ARGO floats, underway sampling along the coast of Ecuador and Peru in collaboration with Ecuadorian and Peruvian colleagues, underway sampling with the shipboard sensors (ADCP, thermosalinograph), and a new towed CTD. Preparations for the DART/Tsunami buoy deployment and of a preliminary report on findings in the Ecuador/Peru coastal region are underway. The towed underway CTD data is shown in Figure 10. A CTD was done (Fig. 11) to 4000 m depth. The profile (Fig. 12) indicates an ocean mixed layer about 70- m thick; note the increased salinity immediately below the mixed layer. Other activities include a launch of an ARGO profiling drifter buoy at 1700 and two surface drifter buoys at 1120 and 2340 GMT.

The ship will remain at the DART buoy location for two days to service the meteorological sensors on the buoy, download data from various sensors, and for buoy-ship intercomparisons. After two days we will depart and head west to the WHOI buoy at 20 S 85 W (est. 1800 on 10/26/2007).

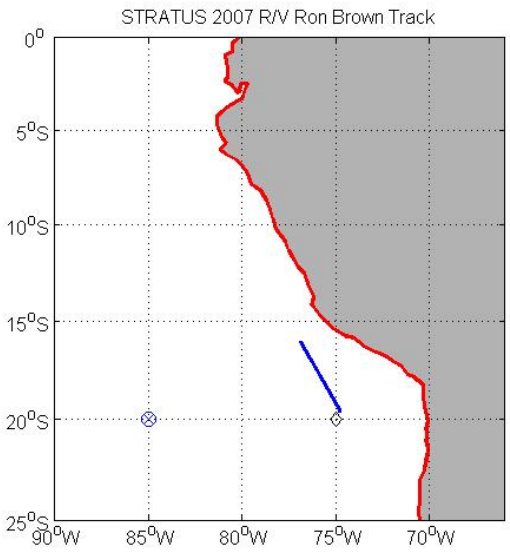

Figure 1. RHB cruise track on JD294 (Oct. 22). The diamond at 75 W is the SHOA tsunami buoy; the circle/plus at 85 W is the WHOI buoy.

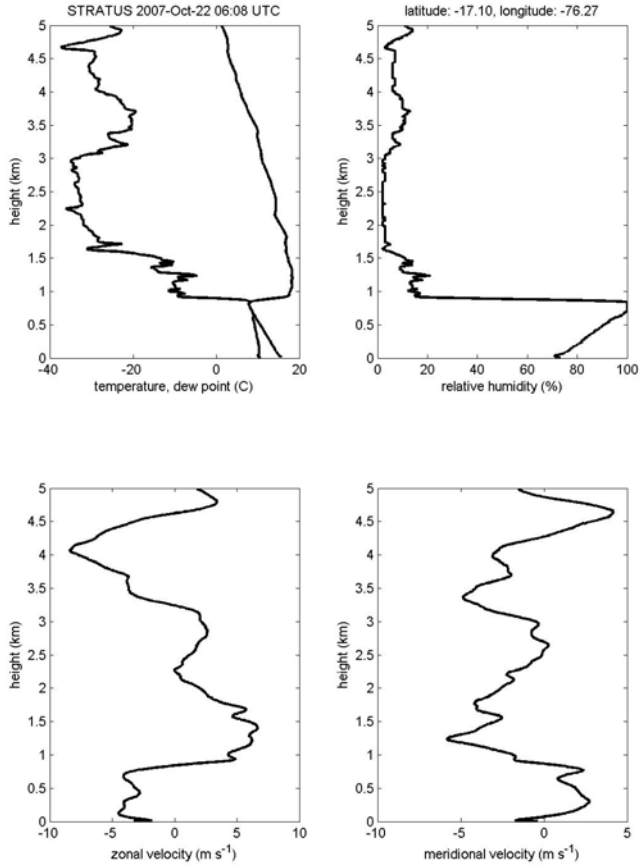

Figure 2. Rawinsonde profile 0600 GMT October 22.

Figure 3. Photograph of stratocumulus clouds 0600 GMT October 22 at 18 S 76 W.

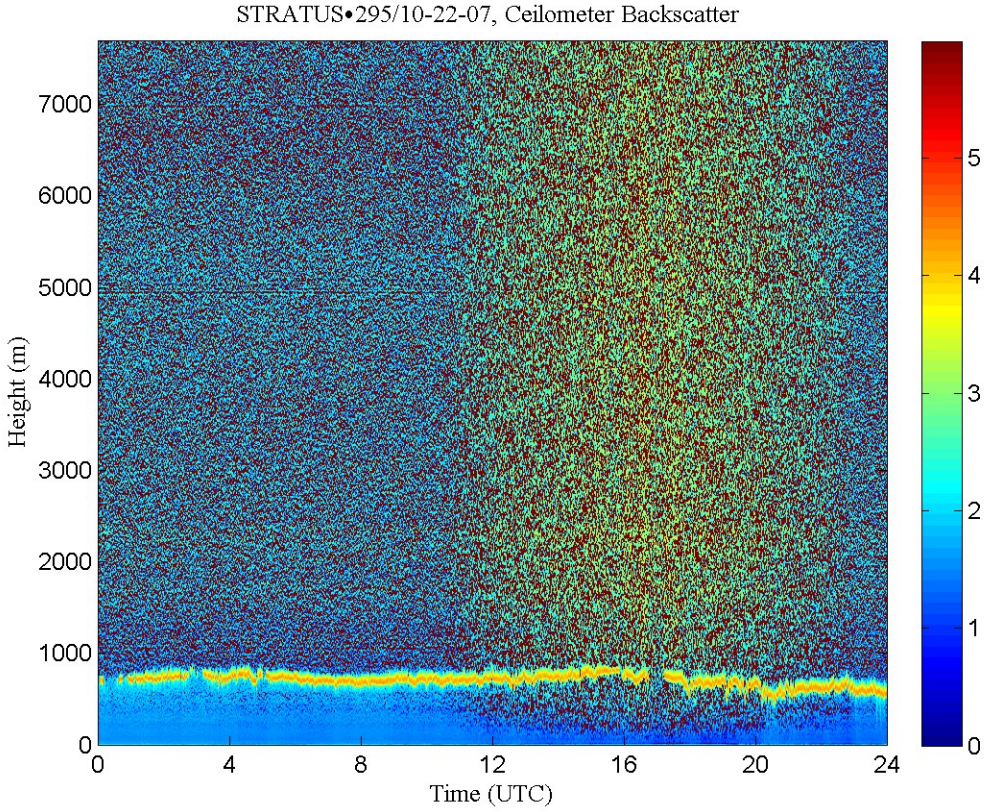

Figure 4. Time height cross section of ceilometer backscatter signal for October 22.

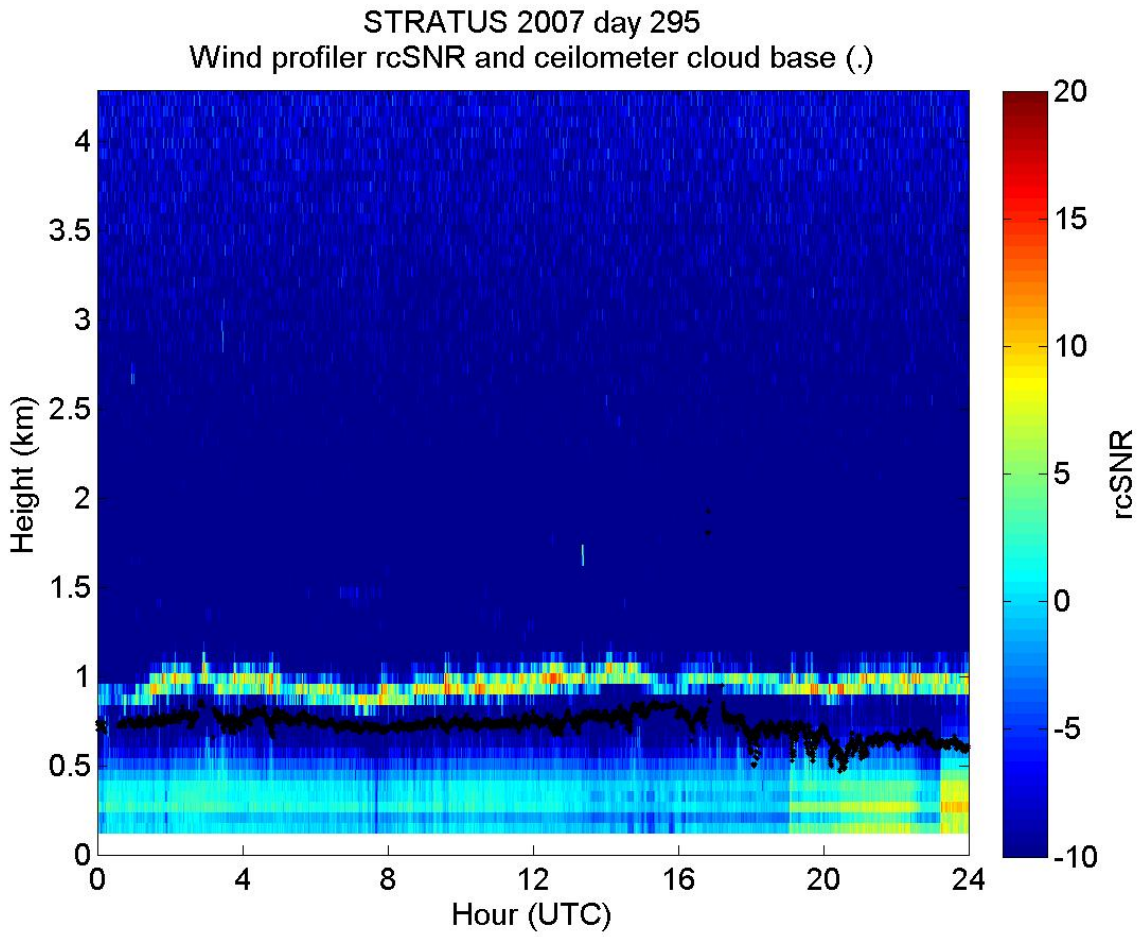

Figure 5. Time height cross section of wind-profiling radar backscatter signal for October 23 (color contours) will ceilometer cloud base heights represented as black dots. The boundary-layer inversion (roughly cloud top height) is apparent as the bright trace at about 1 km height. The stratocumulus cloud occurs between these two heights.

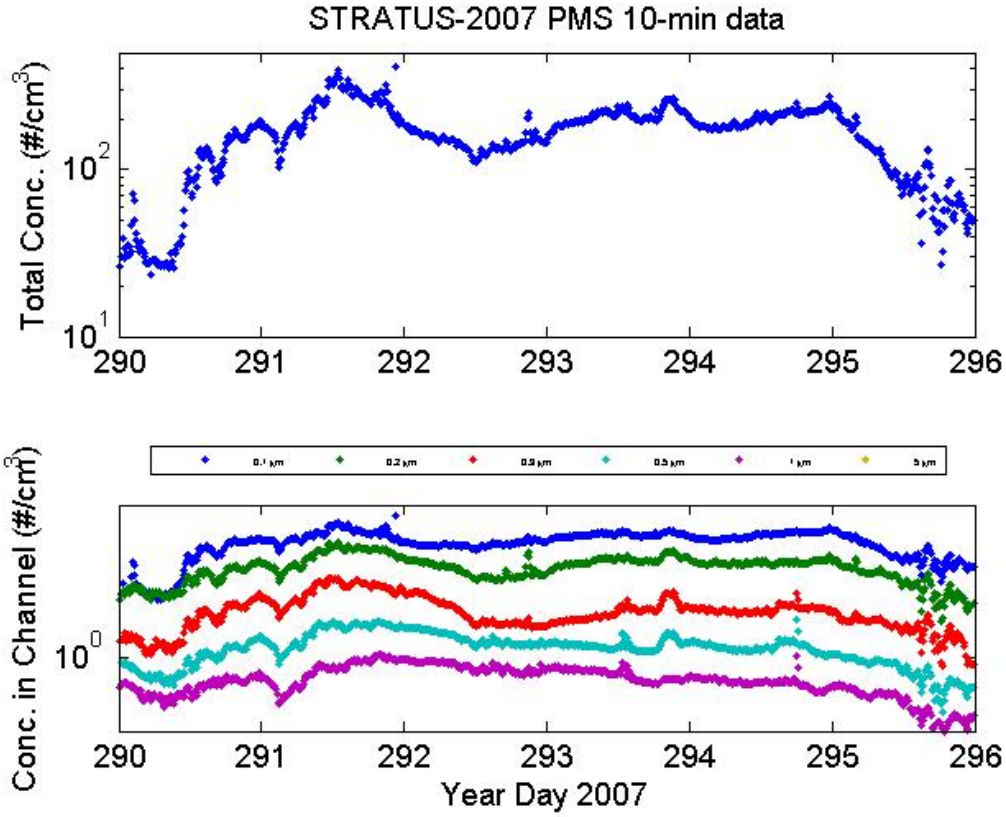

Figure 6. Time series of aerosol concentrations from Oct 17 through October 22. Upper panel: Total concentration for sizes from 0.1 to 5 micrometer. Lower panel: size resolved concentrations.

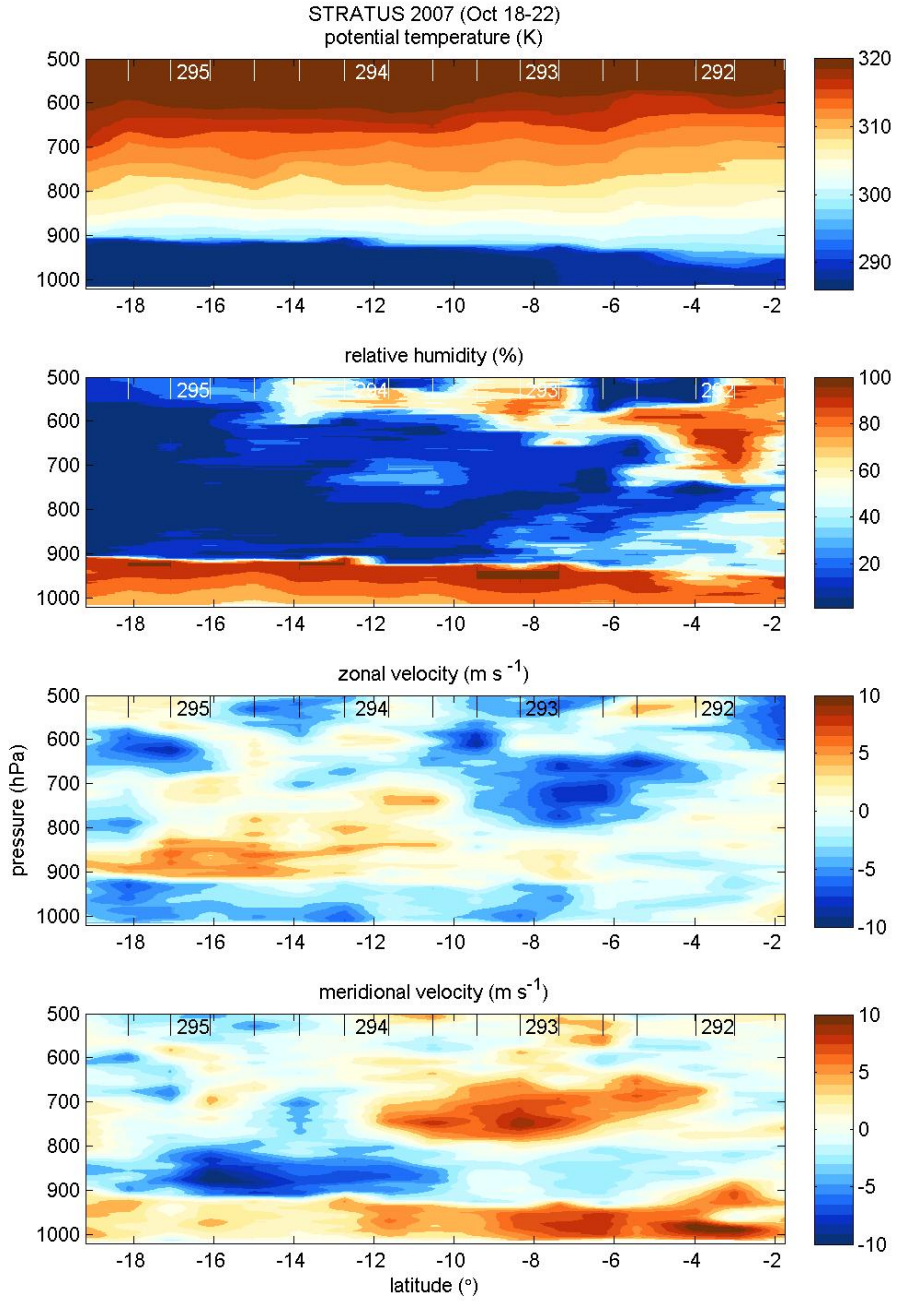

Figure 7. Longitude-height cross section from the rawinsonde data: top panel: temperature; second panel: relative humidity; third panel: zonal wind component; bottom panel: meridional wind component.

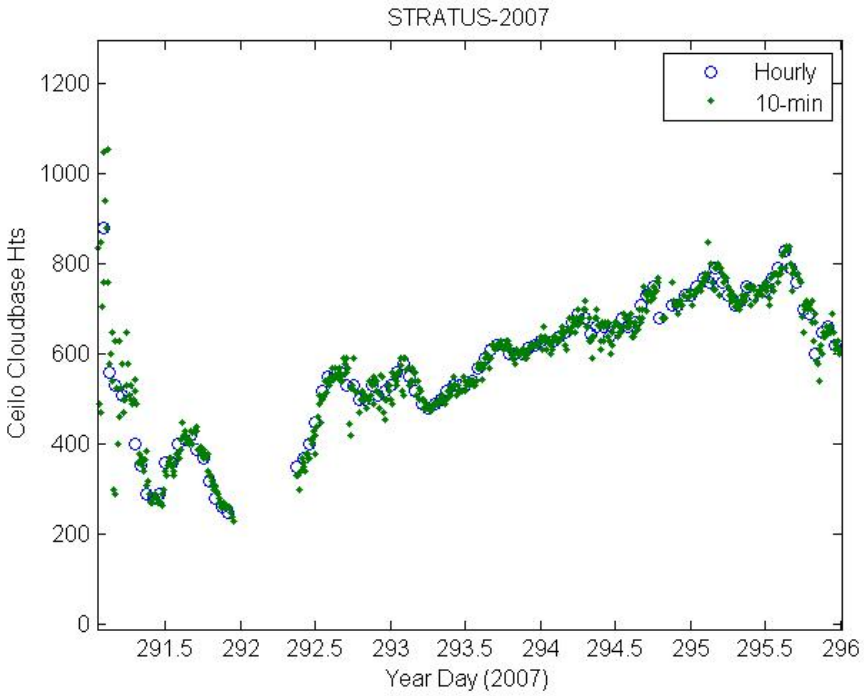

Figure 8. Time-height cross section of cloud base height from the ceilometer.

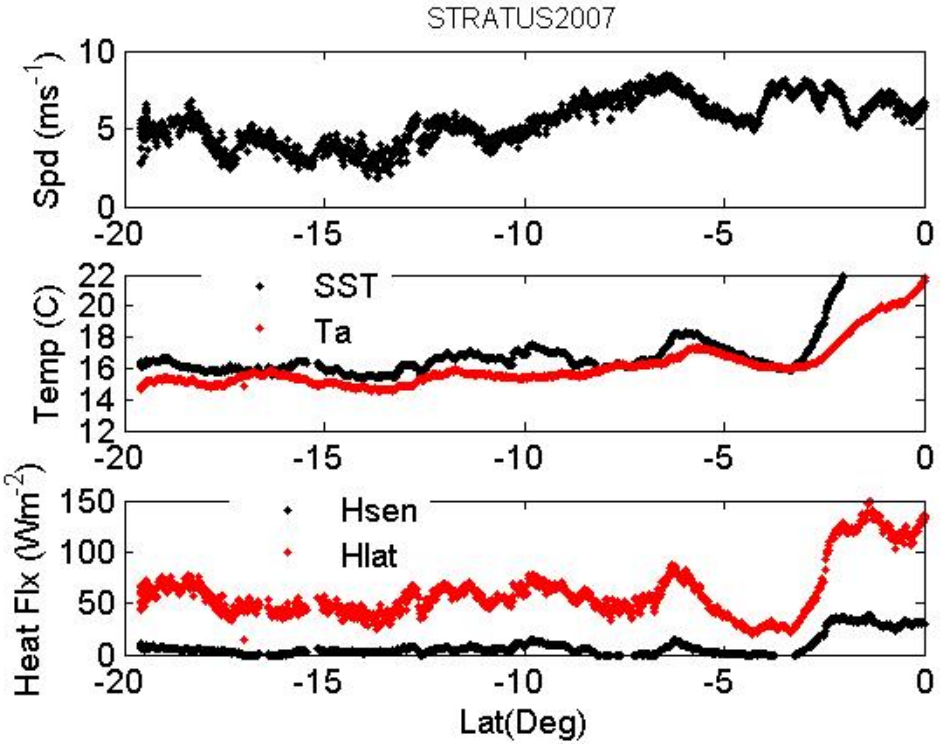

Figure 9. Near-surface meteorological variables as a function of latitude: top panel: wind speed; middle panel: SST (black) and air temperature (red); bottom panel: sensible heat flux (black) and latent heat flux (red).

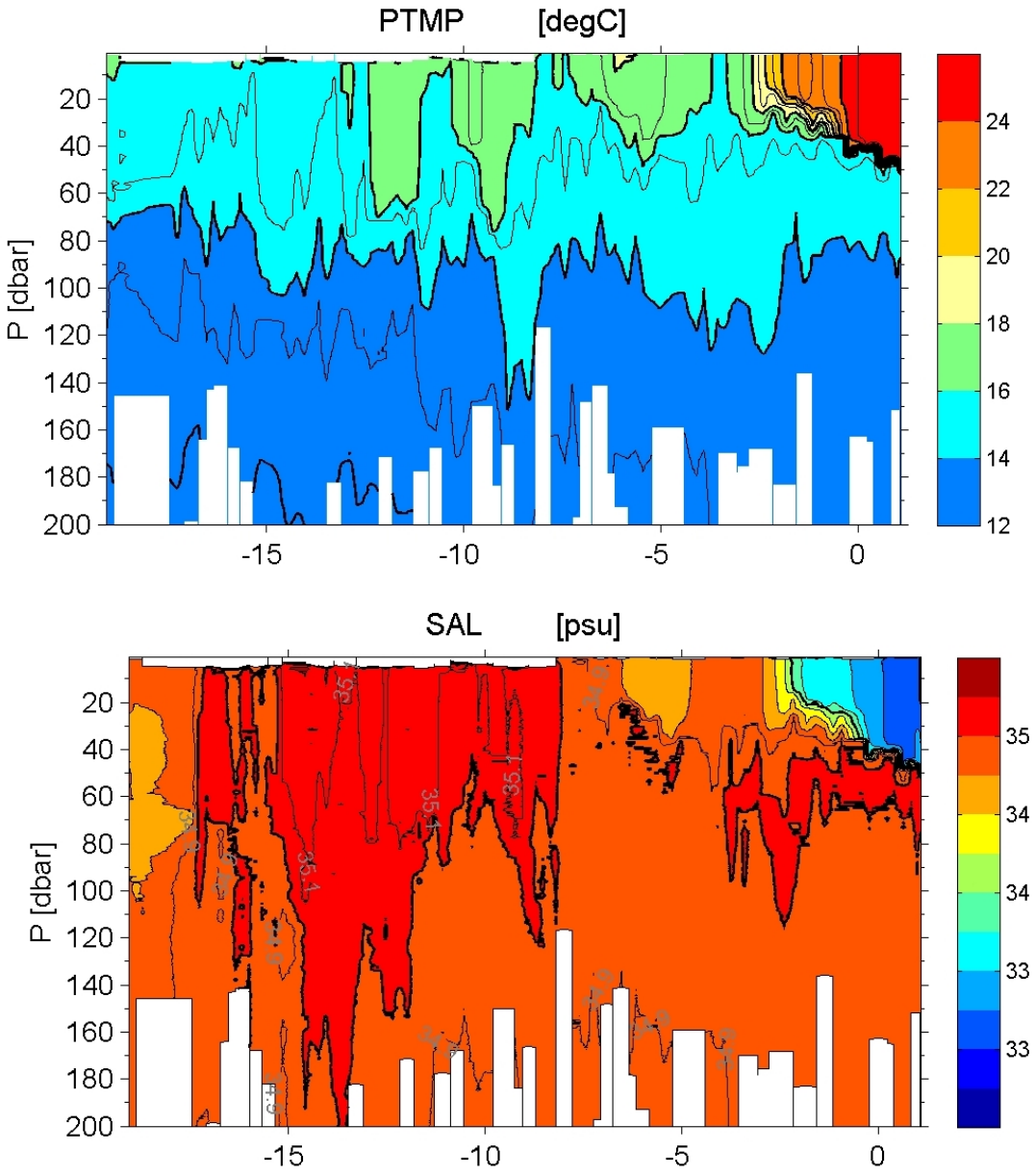

Figure 10. Potential temperature and salinity section along the coast of Ecuador and Peru.

Figure 11. Photograph of CTD just before deployment at 20 S 75 W (L to R: Dana Mancinelli, Jeff Lord, Robert Weller).

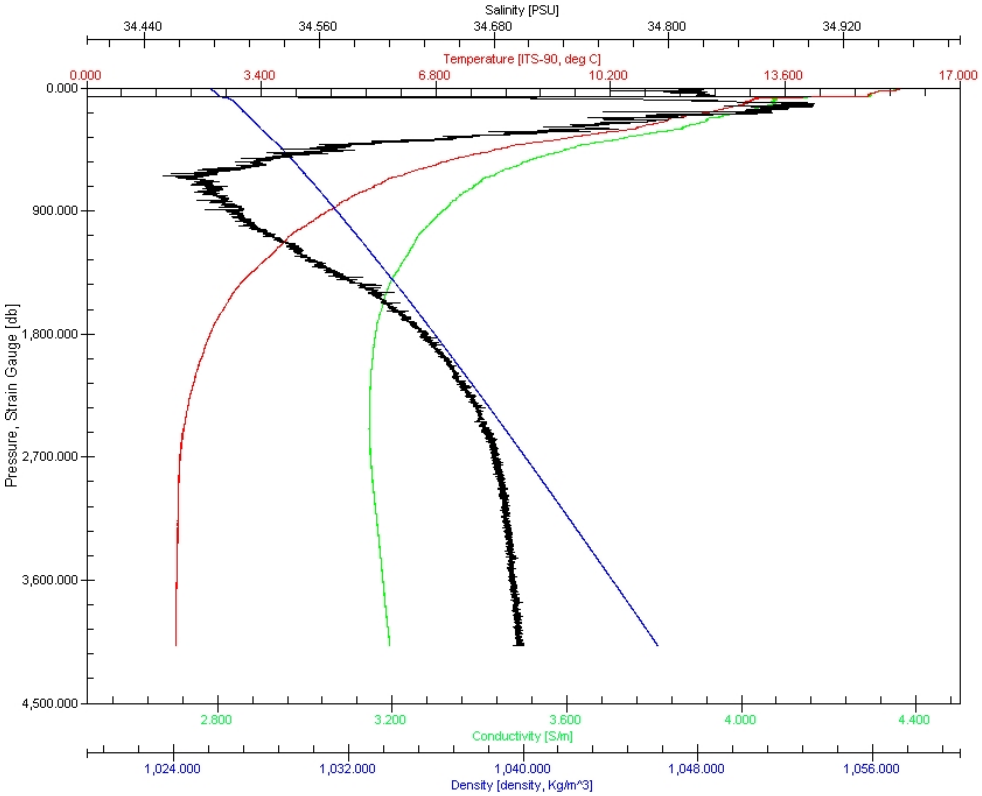

Figure 12. CTD profile from 20 S 75 W: temperature (red), salinity (black), conductivity (green), and density (blue).